PHYSICAL REVIEW B **99**, 161204(R) (2019)

Rapid Communications

Unusual spin properties of InP wurtzite nanowires revealed by Zeeman splitting spectroscopy

D. Tedeschi,[1] M. De Luca,[1,2] P. E. Faria Junior,[3] A. Granados del Águila,[4,*] Q. Gao,[5] H. H. Tan,[5] B. Scharf,[3,†] P. C. M. Christianen,[4] C. Jagadish,[5] J. Fabian,[3] and A. Polimeni[1,‡]

[1]*Dipartimento di Fisica, Sapienza Università di Roma, 00185 Roma, Italy*
[2]*Department of Physics, University of Basel, Klingelbergstrasse 82, 4056 Basel, Switzerland*
[3]*Institute for Theoretical Physics, University of Regensburg, 93040 Regensburg, Germany*
[4]*High Field Magnet Laboratory (HFML – EMFL), Radboud University, NL-6525 ED Nijmegen, The Netherlands*
[5]*Department of Electronic Materials Engineering, Research School of Physics and Engineering, The Australian National University, Canberra, ACT 2601, Australia*

(Received 27 October 2018; published 24 April 2019)

The knowledge of the value and anisotropy of the gyromagnetic factor in semiconducting nanowires (NWs) is crucial for their potential applications in several fields, such as spintronics and topological quantum computation. Here, we present a complete experimental and theoretical investigation of the Zeeman splitting of the fundamental exciton transition in an important material system: wurtzite (WZ) InP NWs. The excitonic g factors are derived by the Zeeman splitting of the spin levels observed by photoluminescence measurements under magnetic fields $\vec{B}$ up to 29 T. In addition to being about three times greater than in zincblende InP, the g factor in the WZ phase is strongly anisotropic (50%) upon variation of the direction of $\vec{B}$ from parallel to perpendicular to the NW axis. Moreover, it exhibits a marked sublinear dependence on $\vec{B}$ whenever $\vec{B}$ points along the NW axis, a feature common to other non-nitride III-V WZ NWs but never properly understood. All these features are well accounted for by a realistic $k \cdot p$ modeling of the Landau levels in WZ InP with the envelope function approximation including excitonic effects. The nonlinearity is spin dependent and due to the coupling between the heavy-hole- and light-hole-like Landau levels. This is indeed a general signature of the bulk WZ structure not requiring quantum confinement nor NW geometry, and is demonstrated to hold also for GaAs, InAs and GaN WZ crystals as reported by Faria Junior *et al.* [Phys. Rev. B, present issue]. Our study solves the outstanding puzzle of the nonlinear Zeeman splitting found in several III-V WZ NWs.

DOI: 10.1103/PhysRevB.99.161204

The spin properties (such as value and anisotropy of the g factor) of semiconducting nanowires (NWs) are extremely important for the research fields of spintronics [1] and topological quantum computation [2]. For instance, in many studies of Majorana bound states based on a semiconductor NW-superconductor heterostructure, the ability to realize the topological phase in the proximitized NW depends on the interplay between the proximity-induced gap and the effective Zeeman energy; this latter quantity being dependent on the NW g factor [2]. Additionally, the g factor is quite sensitive to the changes occurring in the band structure of a crystal upon the interaction with foreign atoms [3]. While the spin properties of III-V NWs with a zincblende (ZB) crystal structure are available from the same material in the bulk form, this is not the case of NWs with the wurtzite (WZ) structure, as WZ has no bulk counterpart in many important III-V semiconductors, such as GaAs, InP, and InAs. Moreover, the g-factor dependence on the relative orientation between $\vec{B}$ and specific crystallographic directions can provide insightful information about the symmetry characteristics of the underlying electronic structure [4–6]. Indeed, in the case of C_{6V} symmetry pertinent to the WZ, the Zeeman split components of the exciton differ considerably depending on the experimental configuration employed [7–9]:

$$\Gamma_5^{\pm} - \mathrm{DS_F} = S \cdot \mu_B |g_{e,\parallel} - g_{h,\parallel}| B, \quad \text{for } \vec{B} \parallel \vec{q} \parallel \hat{c} \text{ (Faraday)}, \tag{1}$$

$$\Gamma_{5/6}^{\pm} - \mathrm{DS_V} = S \cdot \sqrt{\Delta_{56}^2 + \mu_B^2 g_{e,\perp}^2 B^2}, \quad \text{for } \vec{B} \perp \vec{q} \parallel \hat{c} \text{ (Voigt)}, \tag{2}$$

where S is the spin vector component ($S = \pm\frac{1}{2}$), μ_B is the Bohr magneton, $\vec{q}$ is the emitted photon wave vector, $\hat{c}$ is the [0001] axis of the WZ lattice (corresponding to the axial direction in NWs, see insets in Fig. 1), and Δ_{56} is the electron-hole exchange energy separating spin-allowed Γ_5 (bright) and spin-forbidden Γ_6 (dark) excitons [10]. $\Gamma_{5/6}$ is the mixed state resulting when an external perturbation (e.g., a magnetic field) breaks the WZ crystal symmetry [7–9]. Finally, $\mathrm{DS_{F/V}}$ is the exciton diamagnetic shift relative to the Faraday (F, $\vec{B} \parallel \vec{q}$) and Voigt (V, $\vec{B} \perp \vec{q}$) configurations. "e" and "h" refer to electron and hole parameters. Clearly, a linear and quasilinear

*Present address: Division of Physics and Applied Physics, School of Physical and Mathematical Sciences, Nanyang Technological University, Singapore 637371, Singapore.
†Present address: Institute for Theoretical Physics and Astrophysics, University of Wuerzburg, 97074 Wuerzburg, Germany.
‡Corresponding author: antonio.polimeni@roma1.infn.it

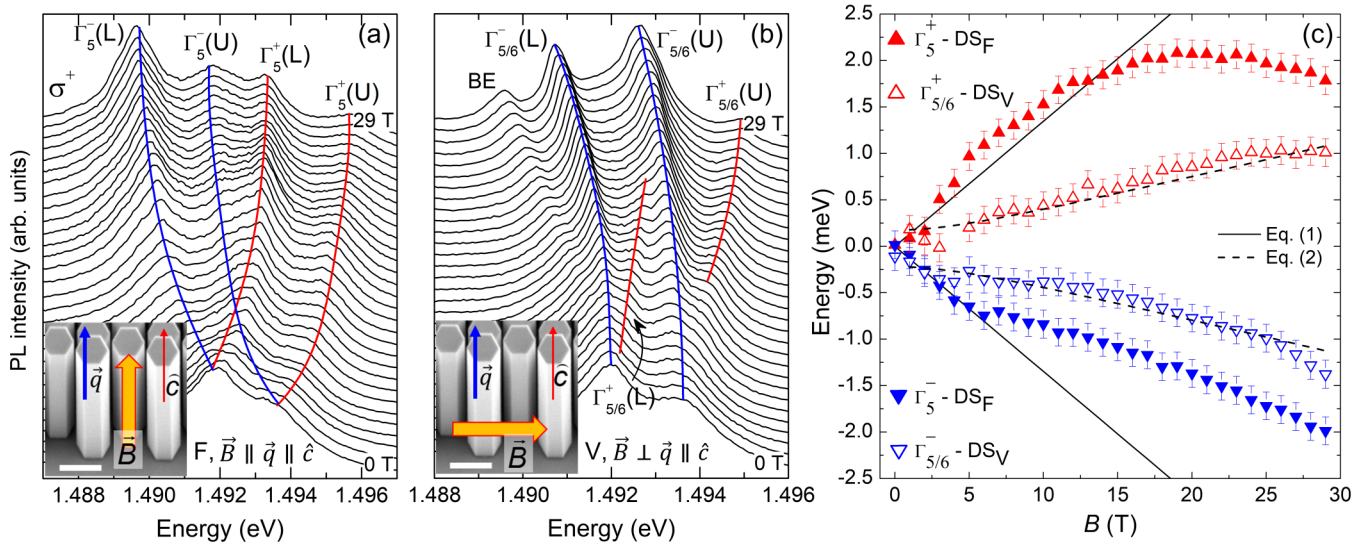

FIG. 1. (a) $T = 4.2$ K photoluminescence spectra of WZ InP NWs from 0 to 29 T in step of 1 T in Faraday geometry ($\vec{B}//\vec{q}//\hat{c}$, inset). The spectra were filtered by σ^+ circular polarization. The different components are indicated by colored lines. Each $B \neq 0$ T spectrum has been redshifted by the corresponding diamagnetic shift. (b) Same as (a) for the Voigt $\vec{B} \perp \vec{q}//\hat{c}$ geometry. Insets: scanning electron microscopy images of the SAE NWs (scale bar is 1 μm) with illustrated experimental geometry. (c) Energy of the free-exciton components displayed in panels (a) and (b) after subtraction of the diamagnetic shift (DS_i; i = F, V): Faraday, full triangles; Voigt, empty triangles. Solid lines are the theoretical values obtained via Eq. (1) with the calculated $|g_{e,\parallel} - g_{h,\parallel}| = 4.66$ in Faraday. Dashed lines are fittings to the data via Eq. (2), using the calculated $g_{e,\perp} = 1.29$ in Voigt.

dependence on B is expected for $\vec{B} \parallel \vec{q}$ and $\vec{B} \perp \vec{q}$, respectively, each being ruled by a different g factor (labeled as $g_\parallel$ and $g_\perp$, respectively). Departures from these behaviors may occur whenever g is field dependent, a case observed in quantum wells and ascribed to the coupling between heavy- and light-hole subbands [11–15]. No similar effects were reported in bulk materials, while a B-dependent g was first observed in WZ NWs (InP, GaAs, and InGaAs) [9,16,17], but never modeled. Since the size ($\geqslant$100 nm) of those NWs rules out the carrier quantum confinement effect, the observation of the B dependence of the g factor has to be attributed exclusively to the WZ phase and not to the NW shape/size.

Here, we measured by magneto-photoluminescence (PL) and modeled with a multi band $k \cdot p$ theory the exciton Zeeman splitting (ZS) in WZ NWs. We focus on InP NWs, which is the NW III-V system where most of the main band structure properties have been best established to date [18]. Magnetic fields up to 29 T were used in Faraday and Voigt geometries. In the latter case, the exciton ZS follows Eq. (2) with $g_{e,\perp}$ in excellent agreement with our theoretical expectations. In the Faraday configuration, instead, the exciton ZS exhibits a strongly nonlinear field dependence that we explain by a model that considers the spatial dependence of the vector potential in the $k \cdot p$ Hamiltonian. In particular, we find that the admixing between wave functions of the A (heavy-hole, HH, like) and B (light-hole, LH, like) valence bands (VBs) characteristic of the WZ lattice leads to the nonlinear behavior, and, surprisingly, the nonlinearity is borne by just one of the two Zeeman split components. This finding can be traced back to the interplay between the symmetry of the VB wave functions and their spin. Finally, we obtain a remarkable quantitative agreement with the experimental data for all geometries by including the excitonic effects. Based on the theoretical framework developed in this manuscript, Faria Junior *et al.* [19] showed that the spin-dependent nonlinear features are indeed a common characteristic for other WZ materials, such as GaAs, InAs, and GaN.

The InP NWs were grown by selective-area-epitaxy (SAE) and by the vapor-liquid-solid (VLS) method. They exhibit nearly pure WZ phase and perfect vertical alignment to the substrates. Details about growth and optical properties of SAE and VLS NWs are in Refs. [9] and [20], respectively. The insets in Fig. 1 show the scanning electron microscopy images of the SAE NWs. These NWs can be regarded as bulk-like materials given their average diameter and height of 650 nm and 5 μm, respectively. For PL measurements, the samples were placed in a Bitter magnet at $T = 4.2$ K using a bath cryostat. PL was excited by a $\lambda = 532$-nm laser (focused to a $\sim$10 μm-diameter spot), collected by the same objective, dispersed by a 0.30-m monochromator, and detected by a Si charge-coupled device. PL circular polarization was analyzed using a liquid crystal variable retarder and a linear polarizer. Theoretical investigation was performed with the $k \cdot p$ method, using the recently reported Hamiltonian and InP WZ parameters [21]. For the linear ZS regime, we calculated the g factors using a perturbative technique similar to the conventional Roth, Lax, and Zwerdling approach [22]. To capture the nonlinear features, we investigated the Landau level (LL) spectra including the spatial dependence of the vector potential [23]. The resulting Hamiltonian was then solved numerically using the finite difference method [24]. The electron-hole Coulomb effects were finally included *via* the Bethe-Salpeter equation (BSE) [25].

The magneto-PL spectra of the WZ InP NWs in the free-exciton (FE) energy region are displayed in Fig. 1. In panel (a) we have $\vec{B} \parallel \hat{c} \parallel \vec{q}$, and the emitted photons are

circularly dichroic, with the Zeeman-split levels being discernable by polarization optics. Γ_5 denotes the symmetry of the bright exciton formed by the conduction Γ_{7C} and valence Γ_{9V} band states of the WZ [26,27]. The spectra are shown only for PL detected selecting σ^+ circularly polarized light for clarity reasons (σ^- detection is shown in Ref. [28]). At zero field, the FE lineshape exhibits a doublet structure caused by the scattering of the excitons with donor impurities [9,29]. These two components [named Γ_5(U) and Γ_5(L) for upper and lower energy, respectively] are regarded as two distinct exciton distributions. With increasing B, Γ_5(U) and Γ_5(L) both shift in energy and split into $\Gamma_5^{\pm}$ Zeeman states (highlighted by solid lines). The corresponding diamagnetic shift (evaluated and discussed in Ref. [9]) has been subtracted to each $B \neq 0$ spectrum to highlight the ZS of the U and L components. In panel (b) we have $\vec{B} \perp \hat{c} // \vec{q}$ and Γ_5 and Γ_6 excitons are mixed by the field and the resultant state is indicated as $\Gamma_{5/6}$ [4,26,27]. Each $B \neq 0$ spectrum has been redshifted by the corresponding diamagnetic shift to focus on the ZS only [9]. Due to the relative orientation between $\vec{B}$ and $\vec{q}$, no PL circular dichroism is observed [4,8,10,26] and circular polarization filtering cannot highlight the ZS. However, the narrow lineshape of the PL bands makes it still clearly visible. Indeed, the PL peaks corresponding to the $\Gamma_{5/6}^{\pm}$ branches are highlighted by solid lines. A bound exciton (BE) is also observed for $B > 10\,\mathrm{T}$ [9]. Notice that in both geometries there is a narrowing of PL bands with increasing B. This is caused by the B-induced quantization of the carriers' energy into LLs, namely, by a modification of the density of states from three-dimensional (3D)- to 1D-like [30–33].

Figure 1(c) shows the field evolution of the Zeeman-split states resulting from the spectra displayed in Figs. 1(a) and 1(b) and evaluated by the spectrum second derivative [9]. In Voigt geometry (open triangles), the Zeeman-split components can be resolved at all fields only for the $\Gamma_{5/6}$(L) exciton distribution. The two $\Gamma_{5/6}^{\pm}$ components shift at the same rate following Eq. (2) at all fields. The dashed lines are fittings to the data with only one free parameter: the electron-hole exchange energy Δ_{56}. We set $g_{e,\perp} = 1.29$, namely the value calculated *via* the 8×8 $k \cdot p$ bulk Hamiltonian for WZ InP [21]. The details regarding the perturbative calculation of the g factors are given in Ref. [28]. The experimental value of $\Delta_{56} = (0.3 \pm 0.2)\,\mathrm{meV}$ is about one order of magnitude larger than in ZB InP [34] indicating an augmented exchange interaction in WZ.

In Faraday configuration, we show the average values of the Γ_5(U) and Γ_5(L) exciton distributions (full triangles). The solid lines are the theoretical ZS evaluated by Eq. (1) with $|g_{e,\parallel} - g_{h,\parallel}| = 4.66$ from $k \cdot p$ calculations [28]. In contrast to the Voigt case, the predicted field dependence is only observed for $B < 5\,\mathrm{T}$. Remarkably, the two opposite spin components determined experimentally show very different field dependences: Γ_5^- is approximately linear, while Γ_5^+ is not pointing to a nonlinear ZS, showing a field-dependent g factor. The presence of a field-dependent g factor solely in Faraday geometry suggests that the valence band states ought to be responsible for such a behavior. Indeed, only in Faraday geometry the hole g factor plays a role in the ZS, as apparent from Eqs. (1) and (2).

In order to describe the nonlinear features observed in Faraday, we must move beyond the linear g factor picture described by the simple Eq. (1). Thus, we use a more general approach combining the $k \cdot p$ method with the envelope function approximation [23,35]. The total *single-particle* Hamiltonian of the system is

$$H_{\mathrm{bulk}}\left[\vec{k} \rightarrow -i\vec{\nabla} + \frac{e}{\hbar}\vec{A}\,(\vec{r})\right] + \frac{\mu_{\mathrm{B}}}{2} g_0 \vec{\sigma} \cdot \vec{B}, \tag{3}$$

where H_{bulk} is the 8×8 $k \cdot p$ bulk Hamiltonian for InP WZ [21], $\vec{A}$ is the vector potential, g_0 is the bare electron g factor, and $\vec{\sigma}$ is the Pauli matrices written in the bulk basis set, i.e., $\vec{\sigma} \cdot \vec{B}$ is the Zeeman term that takes into account only the spins of the bulk Bloch functions. As discussed, we treat the NWs as bulk [36,37]. For a magnetic field the vector potential has a spatial dependence, which we can choose to be only in one dimension for a suitable gauge (for Voigt $\vec{B} = B\,\hat{x} \Rightarrow \vec{A} = B\,y\,\hat{z}$; for Faraday $\vec{B} = B\,\hat{z} \Rightarrow \vec{A} = B\,x\,\hat{y}$). As a consequence, we have two quantum numbers in $\vec{k}$ space: k_B, parallel to $\vec{B}$, and k_A, parallel to $\vec{A}$ and thus the carrier wave vector is two dimensional ($k_y - k_z$ plane for Faraday and $k_x - k_z$ plane for Voigt). This is similar to what happens in the description of a quantum well profile [24,38,39], except that the quantum confinement in our case arises from the spatial dependence of the vector potential. This latter eventually provides the LL spectrum of the system. Because of the multiband character of the bulk Hamiltonian, we cannot find analytical solutions. However, we can obtain the numerical solutions using a finite-difference method in real space [24]. The resulting solution of the Hamiltonian in Eq. (3) gives the LL energies $E_{\mathrm{L}}(k_B, k_A)$ with wave functions ψ_{L,k_B,k_A} . Details of the calculations are in Ref. [28].

Figure 2(a) shows the resulting magnetic field dependence of the topmost and bottommost states of the valence and conduction bands, respectively, in solid colored lines. This dependence is ruled only by the linear shift of the pertinent LLs and by the ZS. Therefore, each LL contains two branches related to opposite spin configurations as highlighted in Fig. 2(a) by short, colored arrows that specify the carrier spin orientation relative to $\vec{B}$ [40].

Conduction band. In both configurations the ZS is linear and the upper (lower) branch has a parallel (antiparallel) spin orientation consistent with positive values of the effective g factors [41].

Valence band. The scenario becomes more complicated, as quite diverse behaviors are observed depending on the configuration:

- Faraday. The state with antiparallel (parallel) orientation has higher (lower) energy, consistent with a negative g factor. Most importantly, the antiparallel state shows a linear dispersion with B, while the parallel state shows a nonlinear dispersion in remarkably good qualitative agreement with the experimental results of Fig. 1(c).

- Voigt. The upper (lower) branch state has a parallel (antiparallel) spin orientation with respect to B [42]. We also point out that a small nonzero and nonlinear ZS ($\sim 0.4\,\mathrm{meV}$ at 30 T) is found despite $g_{e,\perp}$ for HH states should be zero [4], showing that the LL approach describes a richer physics beyond the linear g-factor limit.

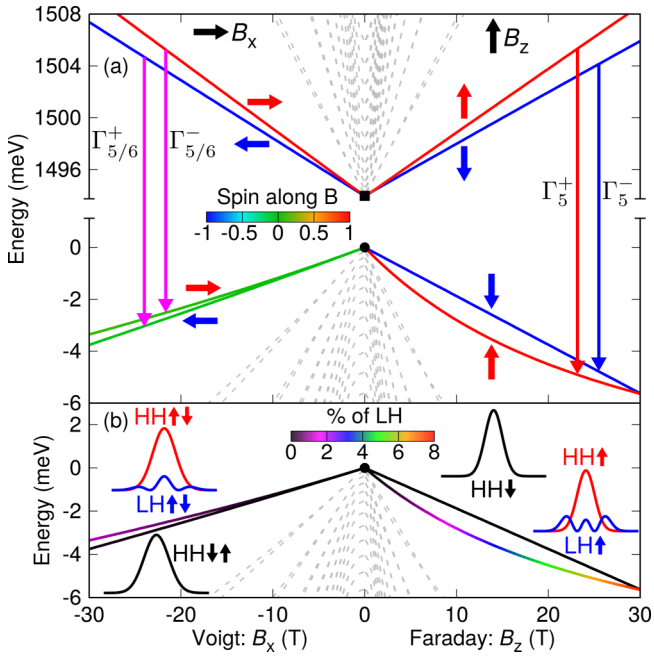

FIG. 2. (a) Calculated energy dispersion as a function of B of the bottom and top most LLs for conduction and valence bands, respectively. Solid, colored lines indicate the first LL. The color code (and short arrows) indicates the spin projection along the field direction. The vertical arrowed lines connect the levels associated to the measured excitonic transitions labeled according to Fig. 1. Dashed, grey lines indicate the higher order LLs that do not play a significant role. (b) Calculated energy dispersion as a function of B of the top most LLs for VBs as in (a). Color code indicates the percentage of LH character of the pertinent valence band LLs. The branches with nonlinear dispersion show a nonzero contribution of LH states that increases with B. The insets show the probability densities of the corresponding levels at 30 T to highlight the peculiar coupling between HH (0 nodes) and LH (2 nodes) LLs. In Faraday (Voigt) geometry the LH probability density is multiplied by a factor of 5 (15).

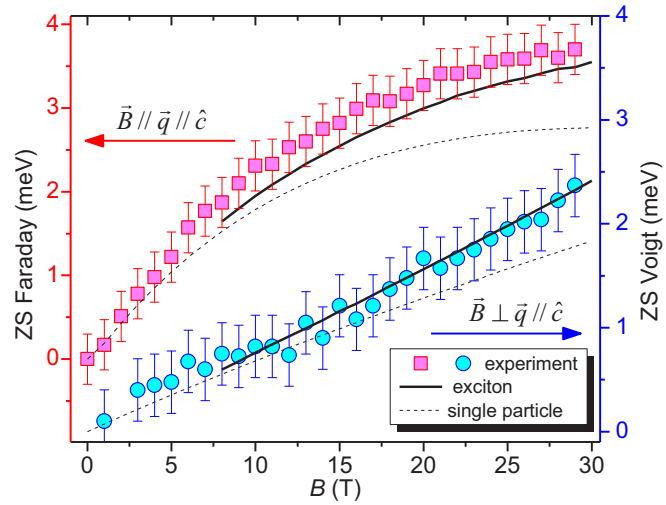

FIG. 3. Experimental exciton ZS in Faraday (squares, left axis) and Voigt (circles, right axis) with calculated ZS either from the single-particle LLs at $k = 0$ (dashed lines) or with exciton effects (solid lines).

It is now important to discuss the origin of the nonlinear dispersion that appears in the VB in both configurations. As shown in Eq. (7) in Ref. [28], the total solution of the coupled set of equations contained in Eq. (3) is a linear combination of wave functions from the bulk energy bands, thus leading to different superpositions for different LLs. Specifically regarding the first LL of the VB, we found that mainly HH and LH contributions remain, so that the LL is a mixing between LH and HH bands. This is the physical origin of the observed nonlinearity. In order to clarify this, we highlight in Fig. 2(b) the calculated contribution of the LH character to the different LL branches: clearly, only for the nonzero contribution of LH are the branches nonlinear [lower (upper) branch for Faraday (Voigt) configuration]. Moreover, such LH contribution increases with magnetic field. At 30 T, there is ∼8%(∼1%) of LH character for the Faraday (Voigt) configuration that indicates the mixing between the HH and LH LLs. The probability densities of the actual wave functions that remain in the superposition of the first LL are given in the inset of Fig. 2(b) for $B = 30$ T.

Therefore, the interplay between the WZ symmetry, embedded in the $k \cdot p$ Hamiltonian, and the break of time-reversal symmetry due to the magnetic field, gives rise to the observed LL dispersion presented in Fig. 2, which is very peculiar for a bulk-like system. In Faraday configuration, the sizeable nonlinear features arise from the LL branch with spin aligned to B. Such a spin-dependent nonlinearity can be understood by looking at the leading terms of the Hamiltonian (specifically, the second order $k \cdot p$ term) [21]. Let us indicate with n the LLs of the single bands (namely, the HH and LH VBs) [43]. In a simple picture, the coupling term between spins up connects HH states (pertinent to band A in WZ), having LL $n = 0$, to LH states (pertinent to band B), having $n = 2$ [see Fig. 2(b)]. For the coupling term between spins down, $n = 0$ HH states are connected to $n = -2$ LH states. Since $n < 0$ are not allowed indices to the LLs, spin-down interactions are suppressed. In Voigt configuration, there is no spin-dependent coupling (both spin components contribute equally) and thus the coupling to the LH state is reduced, hence providing a much smaller nonlinear dispersion than in the Faraday configuration. This explains why Eq. (2) reproduces quite well the Voigt data, while Eq. (1) does not reproduce the Faraday data. To illustrate the coupling between HH and LH states in the presence of magnetic field, we depict an analogy with optical spin orientation in WZ materials [28,44]. This coupling between VB states is indeed a general mechanism that triggers the nonlinearity in other WZ materials, as discussed in Ref. [19].

We move now to the total excitonic ZS obtained in Fig. 1(c) as energy difference between spin components with opposite helicity. In order to provide a reliable comparison to the experimental results, we included the effects of the exciton interaction within the dielectric environment of WZ [45] by numerically solving the effective BSE [25,46], for different values of B (details in Ref. [28]).

The calculated exciton ZS is shown in Fig. 3 (solid lines) in comparison with the experimental data (colored symbols)

and the single-particle LLs (dashed lines) at $\vec{k} = 0$ (extracted from Fig. 2) [47]. The single-particle curve does not consider the effects of nonzero k values, and therefore does not provide the full quantitative account of the data, but still provides excellent qualitative agreement and a clear physical description [48]. Using the robust approach of the effective BSE for excitons, we can reproduce the experimental exciton ZS in Faraday and Voigt geometries very well. Contrasting with the single-particle curve at $\vec{k} = 0$, the exciton calculations probe *via* Coulomb interaction nonzero k values of the band structure that shows different ZS [49]. Ultimately, the Coulomb interaction averages (with particular weights obtained *via* the BSE) the contributions of different k points and consequently brings the values significantly closer to the experimental curve. We emphasize that remarkable agreement is attained without any free parameters. In addition, the same excellent agreement holds also for VLS InP NWs [28].

In conclusion, we presented a full description of the spin properties of WZ InP NWs under external magnetic field. We found a markedly anisotropic g_{exc} in accordance with the symmetry properties of the WZ lattice. In the Faraday configuration, the g_{exc} value is about three times larger than in ZB InP (see our values measured in a InP epilayer [28]) and therefore it becomes as high as in materials with quite a large exciton g factor, such as monolayer WS_2 [50]. Another important difference between WZ and ZB InP is the absence of nonlinearity in the ZS of the ZB exciton, confirmed by our theoretical model [28].

The quantitative agreement between the $k \cdot p$ modeling and experimental ZS data highlighted key aspects regarding the influence of the magnetic field on the excitons in WZ NWs. First, admixing effects between LLs of the A and B VBs occurred at fields as low as 5 T and induced a nontrivial strong bowing of the holes' ZS. Second, the inclusion of the electron-hole Coulomb interaction provided a realistic quantitative account of the experimental data due to the contribution of non-Γ states forming the exciton levels. These properties appear to be general features of WZ crystals and may play a relevant role in several WZ NW systems, which could become the building blocks of topological quantum computers. In fact, such nonlinear features are also present in other WZ materials, for instance InAs, GaAs and even GaN, as shown by Faria Junior *et al.* [19], employing the theoretical approach developed here in this study.

We acknowledge the support of HFML-RU/FOM, a member of the European Magnetic Field Laboratory (EMFL). Part of this work has been supported by EuroMagNET II under the EU Contract No. 228043. D.T. and M.D.L. acknowledge funding by Sapienza Università di Roma under the "Avvio alla Ricerca" grants. A.P. acknowledges financial support from "Awards 2014" and "Ateneo" funding schemes by Sapienza Università di Roma. M.D.L. acknowledges support from the Ambizione grant (Grant No. PZ00P2_179801) by the Swiss National Science Foundation. A.G.D.A acknowledges the financial support of the Presidential Postdoctoral Fellowship program of the Nanyang Technological University. P.E.F.J. and J.F. acknowledge the financial support of the Alexander von Humboldt Foundation, CAPES (Grant No. 99999.000420/2016-06) and SFB 1277 (B05). The Australian authors acknowledge the Australian Research Council for financial support and Australian National Fabrication Facility and Australian Microscopy and Microanalysis Research Facility for providing access to some of the equipment used in this work.

[1] I. Žutić, J. Fabian, and S. Das Sarma, Spintronics: Fundamentals and applications, Rev. Mod. Phys. **76**, 323 (2004).

[2] R. M. Lutchyn, E. P. A. M. Bakkers, L. P. Kouwenhoven, P. Krogstrup, C. M. Marcus, and Y. Oreg, Majorana zero modes in superconductor-semiconductor heterostructures, Nat. Rev. Mater. **3**, 52 (2018).

[3] G. Pettinari, F. Masia, A. Polimeni, M. Felici, M. Capizzi, A. Lindsay, E. P. O'Reilly, P. J. Klar, W. Stolz, G. Bais, M. Piccin, S. Rubini, F. Martelli, and A. Franciosi, Influence of nitrogen-cluster states on the gyromagnetic factor of electrons in $GaAs_{1-x}N_x$, Phys. Rev. B **74**, 245202 (2006).

[4] A. C. Vodina, M. Dietrich, L. Göldner, L. Eckey, A. Hoffmann, A. L. Efros, M. Rosen, and K. B. Meyer, Free excitons in wurtzite GaN, Phys. Rev. B **64**, 115204 (2001).

[5] D. S. Miserev, A. Srinivasan, O. A. Tkachenko, V. A. Tkachenko, I. Farrer, D. A. Ritchie, A. R. Hamilton, and O. P. Sushkov, Mechanisms for Strong Anisotropy on In-Plane g-Factors in Hole Based Quantum Point Contacts, Phys. Rev. Lett. **119**, 116803 (2017).

[6] S. Furthmeier, F. Dirnberger, M. Gmitra, A. Bayer, M. Forsch, J. Hubmann, C. Schüller, E. Reiger, J. Fabian, T. Korn, and D. Bougeard, Enhanced spin–orbit coupling in core/shell nanowires, Nature Commun. **7**, 12413 (2016).

[7] G- L- Bir, B. S. Razbirin, and I. N. Ural'tsev, Exchange interaction and Zeeman effect for an exciton bound to an ionized center in CdSe, Fiz. Tverd. Tela **14**, 433 (1972) [Sov. Phys. Solid State **14**, 360 (1972)].

[8] I. Broser and M. Rosenzweig, Determination of excitonic parameters of the A polariton of CdS from magnetoreflectance spectroscopy, Phys. Rev. B **22**, 2000 (1980).

[9] D. Tedeschi, M. De Luca, A. Granados del Águila, Q. Gao, G. Ambrosio, M. Capizzi, H- H. Tan, P. C. M. Christianen, C. Jagadish, and A. Polimeni, Value and anisotropy of the electron and hole mass in pure wurtzite InP nanowires, Nano Lett. **16**, 6213 (2016).

[10] K. Cho, Unified theory of symmetry-breaking effects on excitons in cubic and wurtzite structures, Phys. Rev. B **14**, 4463 (1976).

[11] N. J. Traynor, R. Warburton, M. J. Snelling, and R. T. Harley, Highly nonlinear Zeeman splitting of excitons in semiconductor quantum wells, Phys. Rev. B **55**, 15701 (1997).

[12] J. Jadczak, M. Kubisa, K. Ryczko, L. Bryja, and M. Potemski, High magnetic field spin splitting of excitons in

asymmetric GaAs quantum wells, Phys. Rev. B **86**, 245401 (2012).

[13] L. K. Castelano, D. F. Cesar, V. Lopez-Richard, G. E. Marques, O. D. D. Couto, Jr., F. Iikawa, R. Hey, and P. V. Santos, Zeeman splitting and spin dynamics tuning by exciton charging in two-dimensional systems, Phys. Rev. B **84**, 205332 (2011).

[14] G. Bartsch, M. Gerbracht, D. R. Yakovlev, J. H. Blokland, P. C. M. Christianen, E. A. Zhukov, A. B. Dzyubenko, G. Karczewski, T. Wojtowicz, J. Kossut, J. C. Maan, and M. Bayer, Positively versus negatively charged excitons: A high magnetic field study of CdTe/$Cd_{1-x}Mg_x$Te quantum wells, Phys. Rev. B **83**, 235317 (2011).

[15] W. Bardyszewski and S- P. Łepkowski, Nonlinear Zeeman splitting of magnetoexcitons in c-plane wurtzite GaN-based quantum wells, Phys. Rev. B **90**, 075302 (2014).

[16] M. De Luca, A. Polimeni, M. Capizzi, A. J. Meaney, P. C. M. Christianen, J. C. Maan, F. Mura, S. Rubini, and F. Martelli, Determination of exciton reduced mass and gyromagnetic factor of wurtzite (InGa)As nanowires by photoluminescence spectroscopy under high magnetic fields, ACS Nano **7**, 10717 (2013).

[17] M. De Luca, S Rubini, M. Felici, A. Meaney, P. C. M. Christianen, F. Martelli, and A. Polimeni, Addressing the fundamental electronic properties of wurtzite GaAs nanowires by high-field magneto-photoluminescence spectroscopy, Nano Lett. **17**, 6540 (2017).

[18] M. De Luca and A. Polimeni, Electronic properties of wurtzite-phase InP nanowires determined by optical and magneto-optical spectroscopy, Appl. Phys. Rev. **4**, 041102 (2017).

[19] P. E. Faria Junior, D. Tedeschi, M. De Luca, B. Scharf, A. Polimeni, and J. Fabian, Phys. Rev. B (to be published).

[20] M. De Luca, A. Polimeni, H. A. Fonseka, A. J. Meaney, P. C. M. Christianen, J. C. Maan, S. Paiman, H. H. Tan, F. Mura, C. Jagadish, and M. Capizzi, Magneto-optical properties of wurtzite-phase InP nanowires, Nano Lett. **14**, 4250 (2014).

[21] P. E. Faria Junior, T. Campos, C. M. O. Bastos, M. Gmitra, J. Fabian, and G. M. Sipahi, Realistic multiband $k\cdot p$ approach from *ab initio* and spin-orbit coupling effects of InAs and InP in wurtzite phase, Phys. Rev. B **93**, 235204 (2016).

[22] L. M. Roth, B. Lax, and S. Zwerdling, Theory of optical magneto-absorption effects in semiconductors, Phys. Rev. **114**, 90 (1959).

[23] C. E. Pryor and M. E. Flattè, Landé g Factors and Orbital Momentum Quenching in Semiconductor Quantum Dots, Phys. Rev. Lett. **96**, 026804 (2006).

[24] S. L. Chuang and C. S. Chang, A band-structure model of strained quantum-well wurtzite semiconductors, Semicond. Sci. Technol. **12**, 252 (1997).

[25] M. Rohlfing and S. G. Louie, Electron-hole excitations and optical spectra from first principles, Phys. Rev. B **62**, 4927 (2000).

[26] H. Venghaus, S. Suga, and K. Cho, Magnetoluminescence and magnetoreflectance of the A exciton of CdS and CdSe, Phys. Rev. B **16**, 4419 (1977).

[27] W. R. Lambrecht, A. V. Vodina, S. Limpijumnong, B. Segall, and B. K. Meyer, Valence-band ordering and magneto-optic exciton fine structure in ZnO, Phys. Rev. B **65**, 075207 (2001).

[28] See Supplemental Material at http://link.aps.org/supplemental/10.1103/PhysRevB.99.161204 for further experimental data under different experimental conditions or on different samples and for an expanded account of the calculations performed.

[29] T. Steiner, M. L. Thewalt, E. S. Koteles, and J. P. Salerno, Effect of neutral donor scattering on the time-dependent exciton-polariton photoluminescence line shape in GaAs, Phys. Rev. B **34**, 1006 (1986).

[30] D. Bimberg, Anomaly of the linear and quadratic Zeeman effect of an effective-mass acceptor: C in GaAs, Phys. Rev. B **18**, 1794 (1978).

[31] B. G. M. Tavares, M. A. Tito, and Yu. A. Pusep, Influence of energy structure on recombination lifetime in GaAs/AlGaAs multilayers, J. Appl. Phys. **119**, 234305 (2016).

[32] G. Pettinari, A. Polimeni, F. Masia, R. Trotta, M. Felici, M. Capizzi, T. Niebling, W. Stolz, and P. J. Klar, Electron Mass in Dilute Nitrides and its Anomalous Dependence on Hydrostatic Pressure, Phys. Rev. Lett. **98**, 146402 (2007).

[33] G. Pettinari, A. Polimeni, M. Capizzi, J. H. Blokland, P. C. M. Christianen, V. Lebedev, V. Cimalla, and O. Ambacher, Carrier mass measurements in degenerate indium nitride, Phys. Rev. B **79**, 165207 (2009).

[34] W. Ekardt, W. Lösch, and D. Bimberg, Determination of the analytical and the nonanalytical part of the exchange interaction of InP and GaAs from polariton spectra in intermediate magnetic fields, Phys. Rev. B **20**, 3303 (1979).

[35] L. C. Lew, Yan Voon, and M. Willatzen, *The $k\cdot p$ Method: Electronic Properties of Semiconductors* (Springer, Berlin, 2009).

[36] P. E. Faria Junior and G. M. Sipahi, Band structure calculations of InP wurtzite/zinc-blende quantum wells, J. Appl. Phys. **112**, 103716 (2012).

[37] L. C. O. Dacal and A. Cantarero, An *ab initio* study of the polytypism in InP, Sci. Rep. **6**, 33914 (2016).

[38] G. D. Sanders and Y.-C. Chang, Theory of photoabsorption in modulation-doped semiconductor quantum wells, Phys. Rev. B **35**, 1300 (1987).

[39] R. Winkler, Excitons and fundamental absorption in quantum wells, Phys. Rev. B **51**, 14395 (1995).

[40] The spin projection is given with respect to the field direction, regardless of Faraday or Voigt configurations: parallel (antiparallel) spin means spin pointing in the same (opposite) direction of B.

[41] In general, g factors are positive if the orbital (and spin-orbital) effects are smaller than the bare carrier g factor, g, so that $g_{\rm tot} = g + g_{\rm orbital} > 0$, in which $g_{\rm tot}$ is the total g factor and $g_{\rm orbital}$ is the orbital (and spin-orbital) contribution. For a more detailed treatment see Eqs. (4) and (5) in Ref. [28].

[42] These branches are green in Fig. 2(a) because the calculated components of the spin along B are very small (0.1 for the upper branch and -0.04 for the lower branch at 30 T), but since the spin projections although small are nonzero, they still have a direction with respect to B, and this direction is represented by the red and blue arrows.

[43] Since n is a quantum number associated with the number of nodes of the wave function of the noninteracting HH and LH LLs, our calculations show that n is equal to 0 for HH (0 nodes) and 2 for LH (2 nodes); see the inset in Fig. 2(b). Thus, in Fig. 2, the first LL pertinent to the valence band consists of a superposition of different ns with different band characters (HH and LH) and thus n is no longer a good quantum number to label the LLs [hence our choice of label L in ψ_{L,k_B,k_A}].

[44] P. E. Faria Junior, G. Xu, Y.-F. Chen, G. M. Sipahi, and I. Zutic, Wurtzite spin lasers, Phys. Rev. B **95**, 115301 (2017).

[45] A. De and C. E. Pryor, Optical dielectric functions of wurtzite III-V semiconductors, Phys. Rev. B **85**, 125201 (2012).

[46] B. Scharf, T. Frank, M. Gmitra, J. Fabian, I. Žutić, and V. Perebeinos, Excitonic Stark effect in MoS_2 monolayers, Phys. Rev. B **94**, 245434 (2016).

[47] For the Voigt configuration we also subtracted the electron-hole exchange energy that is not considered in the present theory.

[48] It is also worth mentioning that although the single-particle description does not provide the best quantitative agreement with the experimental data, it still offers a reliable qualitative behavior that could be used to explore these nonlinear features under different experimental conditions or in different material systems.

[49] For values of magnetic field below 8 T, additional LLs are required to provide a reliable convergence of the excitonic effects, which would drastically increase the computational time without adding new physics to the description. Moreover, we can observe that decreasing the magnetic field the exciton curves converge to the single-particle result.

[50] R. Schmidt, A. Arora, G. Plechinger, P. Nagler, A. Granados del Águila, M. V. Ballottin, P. C. M. Christianen, S. Michaelis de Vasconcellos, C. Schüller, T. Korn, and R. Bratschitsch, Magnetic-Field-Induced Rotation of Polarized Light Emission From Monolayer WS_2, Phys. Rev. Lett. **117**, 077402 (2016).